materials

MDPI

Article

Magneto-Fluorescent Hybrid Sensor $CaCO_3$-Fe_3O_4-$AgInS_2$/ZnS for the Detection of Heavy Metal Ions in Aqueous Media

Danil A. Kurshanov, Pavel D. Khavlyuk, Mihail A. Baranov, Aliaksei Dubavik, Andrei V. Rybin, Anatoly V. Fedorov and Alexander V. Baranov *

Center of Information Optical Technology, ITMO University, 49 Kronverksky Prospekt, 197101 St. Petersburg, Russia; kurshanov.danil@gmail.com (D.A.K.); khavlyuk.stepnogorsk@gmail.com (P.D.K.); mbaranov@mail.ru (M.A.B.); adubavik@itmo.ru (A.D.); rybin@mail.ifmo.ru (A.V.R.); a_v_fedorov@inbox.ru (A.V.F.)

* Correspondence: a_v_baranov@yahoo.com; Tel.: +7-812-457-1781

Received: 31 July 2020; Accepted: 29 September 2020; Published: 30 September 2020

Abstract: Heavy metal ions are not subject to biodegradation and could cause the environmental pollution of natural resources and water. Many of the heavy metals are highly toxic and dangerous to human health, even at a minimum amount. This work considered an optical method for detecting heavy metal ions using colloidal luminescent semiconductor quantum dots (QDs). Over the past decade, QDs have been used in the development of sensitive fluorescence sensors for ions of heavy metal. In this work, we combined the fluorescent properties of $AgInS_2$/ZnS ternary QDs and the magnetism of superparamagnetic Fe_3O_4 nanoparticles embedded in a matrix of porous calcium carbonate microspheres for the detection of toxic ions of heavy metal: Co^{2+}, Ni^{2+}, and Pb^{2+}. We demonstrate a relationship between the level of quenching of the photoluminescence of sensors under exposure to the heavy metal ions and the concentration of these ions, allowing their detection in aqueous solutions at concentrations of Co^{2+}, Ni^{2+}, and Pb^{2+} as low as ≈0.01 ppm, ≈0.1 ppm, and ≈0.01 ppm, respectively. It also has importance for application of the ability to concentrate and extract the sensor with analytes from the solution using a magnetic field.

Keywords: magnetic–luminescent structure; hybrid system; ternary quantum dots; magnetic nanoparticles; iron oxide; calcium carbonate microspheres; sensor

1. Introduction

The industrial development has resulted in constantly increasing levels of heavy metal contamination in the environment [1,2]. To reduce environmental pollution, it is necessary to determine heavy metal ions in soil [3,4] and water resources [5,6]. The detection and selective quantitative definition of heavy metal ions in nature-conservation resources or biological samples have been an important research area for a long time. The development and creation of sensors based on nanoparticles (NPs) have experienced significant growth over the past decades [7–9].

Traditional methods for heavy metal analysis include atomic absorption spectrometry [10,11], inductively coupled plasma mass spectrometry [12,13], and different electrochemical analyses, e.g., potentiometric techniques [14]. However, these methods have complex sample preparation processes, low stability, and are not compatible with different environments, which significantly limits their applicability.

An alternative method is optical detection. The optical research via fluorescence or colorimetric is the most convenient and hopeful method due to its simplicity and high sensitivity of detection [15,16]. In this area, the application of ion-sensitive luminescent quantum dots (QDs) has been of special interest because of different photophysical properties, customizable structures, and the ability to bind to

various ligands, and the possibility integrates into the various hybrid systems with different functional properties while conserving their luminescence properties [17–19].

Many QDs sensor systems are based on binary cadmium compounds, which are hydrophobic toxic compounds [20–22]. Alternative Cd-free nanomaterials are QDs with ternary compositions based on silver or copper, $AgInS_2$, and $CuInS_2$ QDs, which also possess a set of physicochemical properties [23–26] necessary for creating luminescent sensors of toxic compounds. Their photoluminescent (PL) properties are characterized by high quantum PL yield (QYs) ≥ 50% in the visible region from 400 to 1000 nm in the near-infrared (NIR) region after shell growth with, for example, a ZnS semiconductor [24]. Another distinctive characteristic of ternary QDs is broad PL bands with a full width at half-maximum (FWHM) from 100 nm, which slightly overlaps the QD absorption spectrum (Stokes shifts ≈1 eV [27]), in which there is no sharp first exciton peak [28]. Moreover, ternary QDs show long PL lifetimes of some hundred nanoseconds [27,28]. Previous studies demonstrate the possibility of using $AgInS_2$ and $CuInS_2$ QDs in methods for detecting heavy metal ions [29–31].

In addition to detection, it is also important to remove heavy metal ions from the contaminated environment. One of the cleaning methods is sorption using various mesoporous materials, for example, Ca-based materials [32]. Calcium carbonate ($CaCO_3$) crystals are widely used for the manufacturing of carriers containing various embedded nanoparticles or biologically active compounds [33–35]. Nowadays, these $CaCO_3$ crystals (vaterite form) are one of the most popular approaches for matrix formation due to their easy synthesis [36,37], low dispersion, control over crystal size (in the micrometer and submicrometer range [38]), and spherical shape [39], which makes these crystals an attractive candidate for many applications [38,39].

In this work, we focus on the design of $AgInS_2$-based sensors for the most common toxic heavy metal ions, Co^{2+}, Ni^{2+}, and Pb^{2+}, which can accumulate in the human body and cause acute or chronic diseases [40,41]. The sensor is a hybrid complex based on a matrix of porous $CaCO_3$ microspheres doped by Fe_3O_4 magnetic nanoparticles. The surface of the spheres is covered by a shell of several layers of polyelectrolytes. This system combines the properties of several different components, such as the absorption properties of $CaCO_3$ microspheres [42], the photoluminescent properties of $AgInS_2$/ZnS QDs, and the magnetic properties of Fe_3O_4 nanoparticles.

2. Materials and Methods

2.1. Materials

All reagents purchased from Sigma-Aldrich, Steinheim, Germany, were used without further purification. In all procedures, deionized Hydrolab water was used.

To synthesize $AgInS_2$/ZnS QDs, we used indium(III) chloride ($InCl_3$), silver nitrate ($AgNO_3$), zinc(II) acetate dihydrate ($Zn(Ac)_2$), sodium sulfide ($Na_2S{\cdot}9H_2O$), an aqueous solution of ammonia hydrate (NH_4OH), thioglycolic acid (TGA), and isopropyl alcohol.

To synthesize Fe_3O_4 magnetic nanoparticles, we used (tris(acetylacetonato)iron(III)), triethylene glycol (TEG), tetrahydrofuran (THF).

To synthesize $CaCO_3$ microspheres, we used sodium carbonate (Na_2CO_3), calcium chloride ($CaCl_2$), poly(sodium 4-styrenesulfonate) sodium salt (PSS, Mw = 70 kDa) and poly(allylamine hydrochloride) (PAH, Mw = 70 kDa).

The aqueous solutions of heavy metals were prepared by dissolving the salts of metals (cobalt(II) nitrate, nickel(II) sulfate, lead(II) chloride) in water.

2.2. Methods

2.2.1. Synthesis of Fe_3O_4 Nanoparticles

The magnetic Fe_3O_4 nanoparticles were prepared by mixing iron (III) triacetylacetonate and TEG. In the synthesis, 1 mmol of iron precursor and 24 mL of triethylene glycol were added to a three-necked

flask under magnetic stirring. The mixture was degassed at up to 90 °C and kept for 60 min under vacuum. After degassing and flushing with argon, the solution was heated to 275 °C and kept for 2 h under a constant Ar flow. After the synthesis, the NCs were washed with THF by centrifugation and then dissolved in water for storage.

2.2.2. Synthesis of $AgInS_2$/ZnS QDs

For the synthesis of $AgInS_2$ quantum dot cores, 1 mL of $AgNO_3$ water solution (0.1 M), 2 mL of TGA water solution (1.0 M), and 0.2 mL of NH_4OH (5.0 M) water solution were added to 92 mL of water under magnetic stirring and ambient conditions. Then, 0.45 mL of NH_4OH solution (5.0 M) and 0.9 mL of $InCl_3$ water solution (1.0 M) containing 0.2 M HNO_3 were added. After that, the solution changed its color from yellow to colorless. After adding 1 mL of 1.0 M Na_2S water solution (1.0 M), the resultant solution was heated at 95 °C for 30 min by a water bath. For ZnS shell growth on the surface of $AgInS_2$, 1 mL of TGA solution (1.0 M) and 1 mL of $Zn(Ac)_2$ solution (1.0 M) containing 0.01 M HNO_3 was added.

After the synthesis, the $AgInS_2$/ZnS quantum dot solution was cooled and concentrated using rotary evaporation. For the size-selection procedure, the aggregation of quantum dots was initiated by adding 0.5 mL of isopropyl alcohol and subsequent centrifugation at 10,000 rpm for 5 min. The precipitate was separated and marked further as fraction #1. This procedure was repeated until the solution was fully discolored. Here, we used quantum dots with a luminescence peak at ≈600 nm.

2.2.3. Preparation of $CaCO_3$-Fe_3O_4-$AgInS_2$/ZnS (CFA) Fluorescent Sensor

Na_2CO_3 (0.33 M; 700 µL), $CaCl_2{\cdot}2H_2O$ (0.33 M; 700 µL), and Fe_3O_4 nanoparticles (50 µL concentrated aqueous solution) were added to a round-bottom flask. The resulting solution was stirred for 30 s, after which the resulting spheres were centrifuged for 40 s at 3000 rpm. Then, precipitated $CaCO_3$-Fe_3O_4 microspheres were washed twice with H_2O.

The next step was to extend the shell using the Layer-by-Layer (LbL) method. First, 1 mL of PAH solution (6 mg/mL, 0.5 M NaCl, and pH 6.5) was added to the precipitated $CaCO_3$-Fe_3O_4 spheres. The resulting dispersion was shaken for 10 min. Excess polyelectrolyte was removed by washing with water and centrifuging (30 s at 4000 rpm). The procedure was repeated twice. Then, the procedure was repeated using PSS solution (6 mg/mL, 0.5 M NaCl, and pH 6.5). After triple coating with polymer layers (PAH/PSS/PAH), 100 µL of a QDs stock solution was added to the spheres. The dispersion was shaken for 10 min. The excess QDs, by analogy with polyelectrolytes, were centrifuged and washed with water. After the QDs layer, a double layer of PSS and PAH was applied to the spheres.

The resulting fluorescent sensors based on $CaCO_3$ microspheres were dispersed in water.

2.3. Equipments

A spectrophotometer UV-3600 (Shimadzu, Kyoto, Japan) and spectrofluorometer FP-8200 (Jasco, Tokyo, Japan) were used for recording the absorption and PL spectra of the samples, respectively. The SEM and STEM images of the studied samples were taken with a Merlin (Zeiss, Oberkochen, Germany) scanning electron microscope while a FEI Titan electron microscope operating at a voltage of 300 kV was used for getting the TEM image of Fe_3O_4 nanoparticles. The transmitted light images were obtained with a LSM-710 (Zeiss, Oberkochen, Germany) laser scanning confocal microscope equipped with a microobjective of NA = 0.95. The photoluminescence (PL) decay curves of the sample were obtained with a laser scanning confocal microscope MicroTime 100 (PicoQuant, Berlin, Germany) equipped with a pulsed light source with the 80 ps pulses at a repetition rate of 0.2 MHz and a Time Correlated Single Photon Counter (TCSPC) detector. The size of magnetic nanoparticles was determined by dynamic light scattering (DLS) using a Malvern Zetasizer Nano (Malvern, Worcestershire, UK).

3. Results

The formation of the CFA fluorescent sensor was produced (made) in two steps (scheme Figure 1a). In the first step, the $CaCO_3$-Fe_3O_4 microspheres have been formed by using concentrated aqueous solutions of Na_2CO_3 and $CaCl_2$ and magnetic Fe_3O_4 nanoparticles of 5–6 nm mean size. Magnetic Fe_3O_4 nanoparticles are located inside the pores of $CaCO_3$ spheres providing a brownish color of $CaCO_3$-Fe_3O_4. The SEM (STEM) images of $CaCO_3$ microspheres, doped by Fe_3O_4 nanoparticles, Fe_3O_4 magnetic nanoparticles, and $AgInS_2$/ZnS QDs stabilized with TGA are shown in Figure 1b–d, respectively.

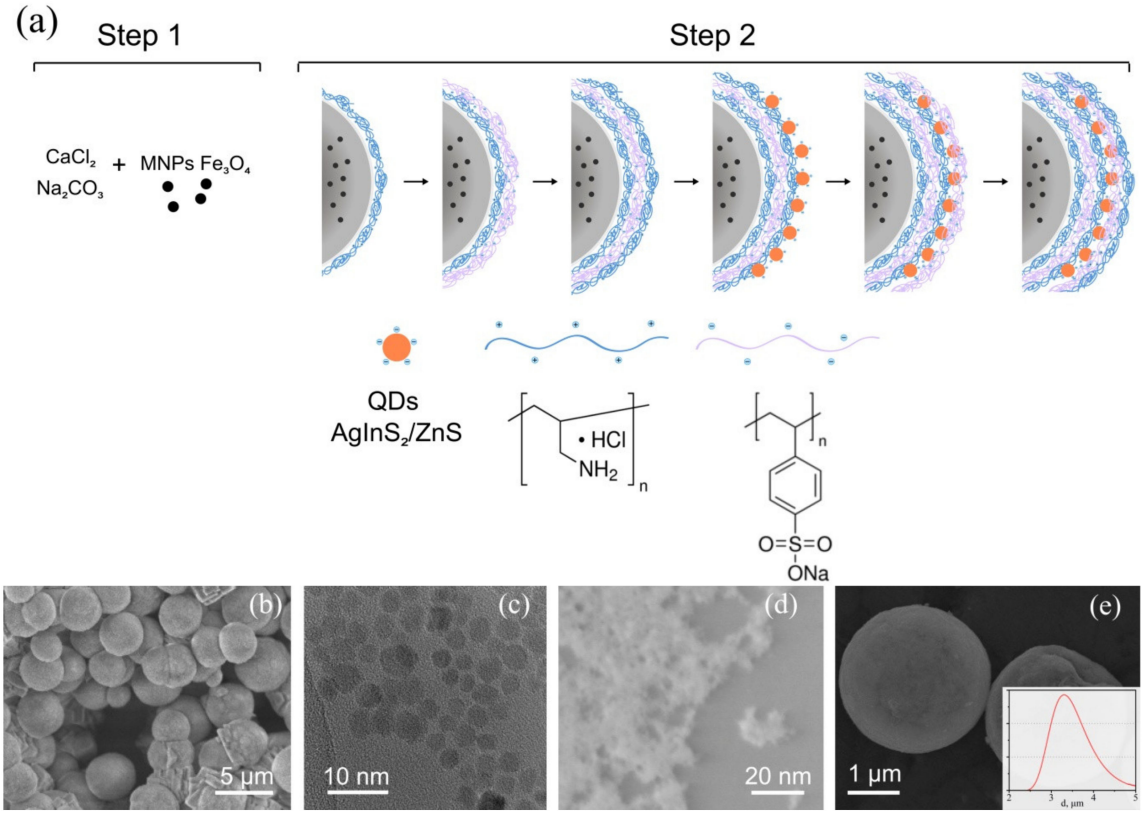

Figure 1. (**a**) Scheme of a two-stage synthesis of a magnetic luminescent sensor based on $CaCO_3$ microspheres, (**b**–**e**) SEM and STEM images of the sensor components: (**b**) $CaCO_3$ microspheres, doped by Fe_3O_4 nanoparticles, (**c**) Fe_3O_4 magnetic nanoparticles, (**d**) $AgInS_2$/ZnS quantum dots (QDs) stabilized with thioglycolic acid (TGA), (**e**) CFA ($CaCO_3$-Fe_3O_4-$AgInS_2$/ZnS) microspheres with polyelectrolyte shell poly(allylamine hydrochloride)/poly(sodium 4-styrenesulfonate) (PAH/PSS). Inset in (**e**) shows a typical dynamic light scattering (DLS) size-distribution plot.

The resulting CFA microspheres with polyelectrolytic shell PAH/PSS were characterized by scanning electron microscopy, DLS, UV-Vis, and photoluminescent steady-state and transient microscopy. Their SEM images are presented in Figure 1e and show spherical microparticles with a mean size of ≈4 μm. DLS measurements showed that an average hydrodynamic diameter of the $CaCO_3$-Fe_3O_4 microsphere is about 3.5–4 μm as determined from the analysis of the size-distribution profile (Figure 1e, inset).

The next step was the formation of polyelectrolyte multilayers and the deposition of the QDs layer on a surface of the microspheres by LbL method. Oppositely charged electrostatically interacting polymers and QDs have deposited alternately on the surface of microspheres [43–45]. In this work, we used PAH and PSS polymers and QDs $AgInS_2$/ZnS core/shell capped with the hydrophilic ligand TGA. To heighten the PL properties and stability of the $AgInS_2$ cores, the cores were passivated by a protective ZnS shell. The resulting stable solution QDs $AgInS_2$/ZnS core/shell had a mean size of ≈5 nm and with a PL QY 30%. At first, two double layers of PAH/PSS polyelectrolytes were deposited on the surface of

$CaCO_3$-Fe_3O_4; then, $AgInS_2$/ZnS QDs were applied over the first layers of the polyelectrolytes shell by electrostatic adsorption using the LbL method. Finally, an additional protective PAH/PSS double layer was placed on the microsphere surface. The resulting CFA fluorescent sensor is illustrated in Figure 1e.

The optical and magnetic properties of the CFA microspheres are illustrated in Figure 2.

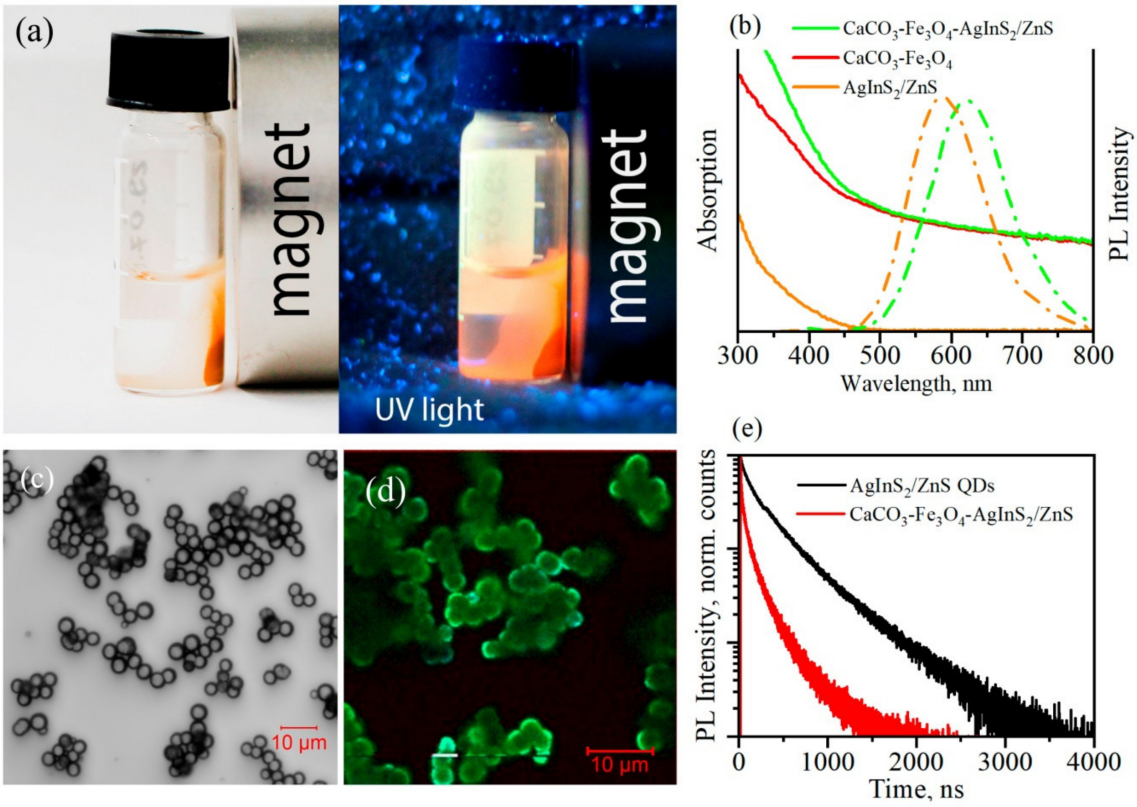

Figure 2. Optical and magnetic properties of the CFA fluorescent sensor. (**a**) Photos of the accumulation of the microspheres to magnetic bar under UV light, (**b**) Absorption (solid line) and photoluminescent (PL) (dash/dotted line) spectra of the CFA fluorescent sensor and $AgInS_2$/ZnS QDs in water (orange $AgInS_2$/ZnS QDs, red $CaCO_3$-Fe_3O_4 microspheres, and green CFA fluorescent sensor), (**c**) Confocal transmitted light images of the CFA microspheres, (**d**) Fluorescence-Lifetime Imaging Microscopy (FLIM) images of the CFA microspheres, (**e**) PL decay curves of the CFA microspheres and the aqueous dispersion of the initial $AgInS_2$/ZnS QDs. The PL measurements shown in panels (**b**–**e**) were done at 350 nm excitation.

The magneto-fluorescent properties of CFA allow easily concentrating sensors with a magnet or detect their PL under ultraviolet light, as shown in Figure 2a.

The absorption spectra of the $AgInS_2$/ZnS QDs, the $CaCO_3$-Fe_3O_4 microspheres, and fluorescent CFA sensors are shown in Figure 2b. It is seen that the absorption spectrum of $CaCO_3$-Fe_3O_4 microspheres contains a noticeable contribution from elastic scattering, which is caused by the rather large size of the microspheres. The absorption of $AgInS_2$/ZnS QDs is characterized by a broad and peak-less spectrum with the absorbance increasing gradually in the shortwave region. The absorption spectra of $CaCO_3$-Fe_3O_4 microspheres and $AgInS_2$/ZnS QDs additively contribute to the absorption spectrum of the CFA microspheres.

The PL spectra of the CFA microspheres and the $AgInS_2$/ZnS QDs in aqueous solution are shown in Figure 2b. This PL spectrum demonstrates a broad and symmetric luminescence band in the visible and NIR region, similar to that of the $AgInS_2$/ZnS QDs in water. Inclusion of the $AgInS_2$/ZnS QDs into polymer layers on the surface of $CaCO_3$-Fe_3O_4 microspheres leads to a small redshift of the PL band as compared to that in solution, which is most likely due to the interaction between close QDs. Confocal

transmitted light and FLIM images of the CFA microspheres presented in Figure 2c,d, respectively, show that luminescent QDs are embedded in the surface layer of the microspheres of about 3–4 μm in diameter, demonstrating bright PL response.

As in the case of the $AgInS_2$/ZnS QDs in the solution, the PL decay of the QDs in the CFA microspheres is characterized by multiexponential decay kinetics, which is a characteristic property of the PL of ternary QDs that originates from the complicated structure of the low-energy states of the $AgInS_2$ QDs [46]. At the same, an average PL lifetime, calculated by the formula:

$$<\tau> = \Sigma A_i \tau_i^2 / \Sigma A_i \tau_i,$$

where A_i is the amplitude and τ_i is the decay time of the i-th exponent, which for the embedded QDs of about 200 ns is remarkably smaller than that of 350 ns for the QDs in aqueous solution. This difference that is seen in Figure 2e shows that embedding QDs in the surface layer of microspheres results in the appearance of the nonradiative channel of the PL decay.

To demonstrate the ability of our fluorescent sensor for the optical detection of heavy metal ions Co^{2+}, Ni^{2+}, and Pb^{2+}, aqueous metal solutions with a concentration of 0.001 M were prepared. To the CFA solution with a volume of 100 μL per 3 mL of water, metal salt solutions were added with a volume of 3 to 300 μL. Then, the optical properties of the CFA in the presence of heavy metal ions were studied.

The results presented in Figure 3 show that the photoluminescence intensity decreases with an increase in the concentration of heavy metals ions. It is not surprising, since the core–shell $AgInS_2$/ZnS QDs has the stabilizer of thioglycolic acid, which forms the negatively charged layer on the surface of the nanocrystals. The quenching of the PL is observed due to the Coulombic interaction of positively charged metal ions from the analyte with the negative organic shell [47]. Data on the ion concentration dependence of the QD PL are reproduced in three independent experiments, which are reflected in values of corresponding PL intensity measurement errors in the right panels of Figure 3. With low concentrations of Co^{2+} ions, a significant decrease in the luminescence intensity of the sensor is observed (Figure 3a). These suggest a high sensitivity of the fluorescent sensor for Co^{2+} ions. The sensitivity of the sensor for Ni^{2+} and Pb^{2+} was lower by an order of magnitude (Figure 3b,c, respectively). Inserts in Figure 3 (right panel) show in detail the measured PL reduction with the addition of the smallest amount of the Co^{2+}, Ni^{2+}, and Pb^{2+} ions. A simple estimation of low limits of ion concentrations in solution by measuring the reduction of the sensor PL intensity as compared with the ion-free solution within experimental errors of ≈1–2%, gives concentrations of 10^{-8} M Co^{2+} and 10^{-7} M Ni^{2+} and Pb^{2+} even without optimization of the sensor parameters. These values are close to the detection limit reported in [48] for a dissociative CdSe/ZnS QD/PAN complex for luminescent sensing of metal ions in aqueous solutions and orders of magnitude higher for Co(II) and for Ni(II) obtained by colorimetric (absorption) measurements with 1-(2-pyridilazo)-2-naphtol (PAN) as a complexing reagent in the aqueous phase using the non-ionic surfactant Tween 80 [49]. The difference in the luminescence extinguishing of ternary quantum dots by Co^{2+}, Ni^{2+}, and Pb^{2+} is not quite understood at the moment and is the subject of consideration.

At the same time, it should be noted that despite the good sensitivity, the proposed fluorescent sensor does not exhibit selectivity for ions recognition. Therefore, its practical use is limited by a quick on-line preliminary analysis of the presence of heavy metal ions in water samples and a recommendation for further detailed analysis of the elemental composition of ions.

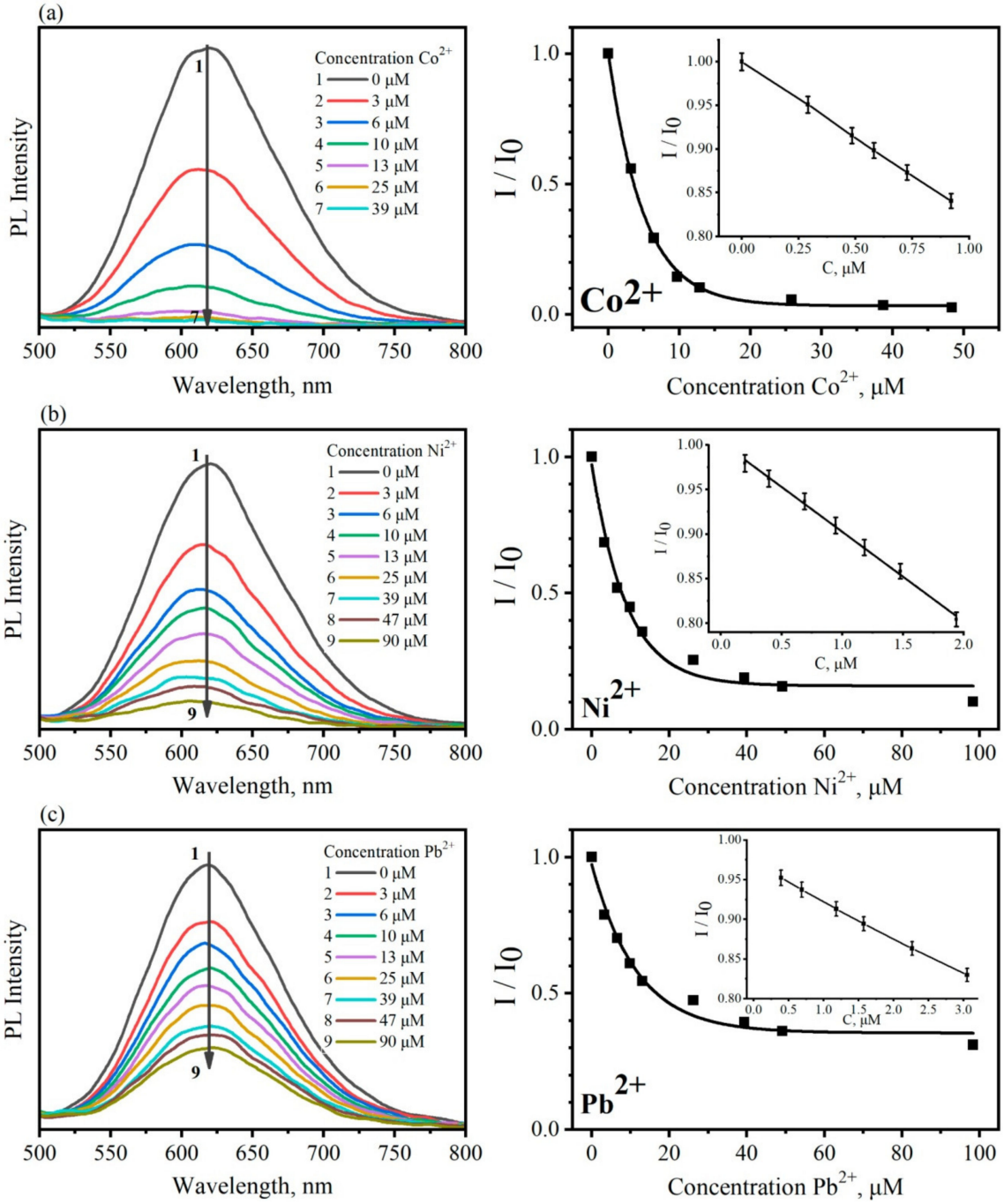

Figure 3. Quenching the CFA sensor luminescence upon increasing concentration heavy metal ions in aqueous solution. Left panel—PL band of CFA sensors as a function of the concentration of the Co^{2+}, Ni^{2+}, and Pb^{2+} ions. Right panel—integrated luminescence intensity ratio (I_0/I) dependence on the concentration of heavy metal ions for (**a**) Co^{2+}, (**b**) Ni^{2+}, (**c**) Pb^{2+}; insets show the regions of low ions concentration.

Due to the presence of magnetic Fe_3O_4 nanoparticles in the microspheres, the sensor with absorbed metal ions can be removed from the solution using a magnetic field, for example, for further analysis of the chemical and/or elemental composition of toxic impurities. To demonstrate this phenomenon, the 20 μL of a 0.001 M aqueous solution of Co^{2+} ions was added to the sensor based on CFA microspheres. In this case, a decrease up to 35% of the initial value was observed in the intensity of the photoluminescence of the sensor (Figure 4b). After the sensor was removed from the test solution using a magnet, the purified solution was again analyzed using the CFA sensor at the

same amount (Figure 4c–d). The intensity of luminescence was practically unchanged compared to the solution without metal ions and it decreased by 15%, which indicates a significant decrease in the content of metal ions. This result suggests that the microspheres were successfully absorbed by the heavy metal ions Co^{2+} in solution.

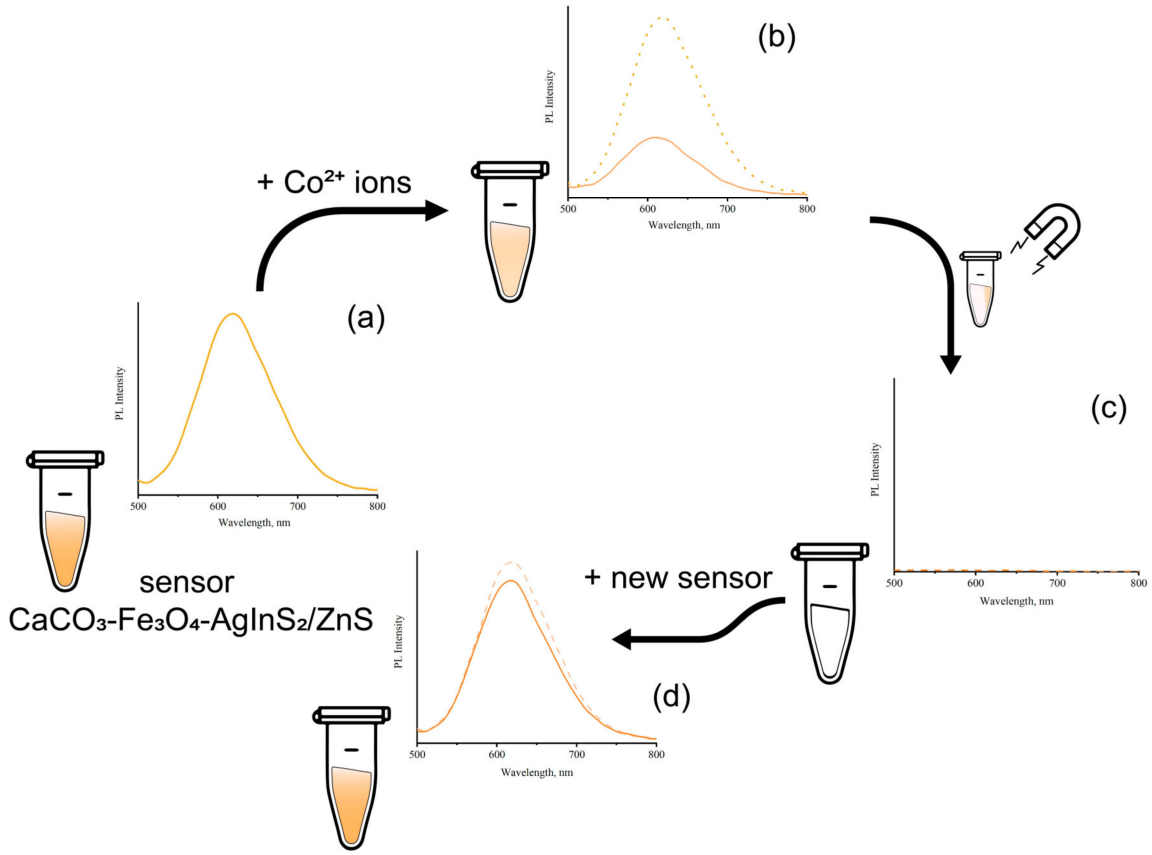

Figure 4. (**a**) PL spectra of the CFA fluorescent sensor without heavy metal ions, (**b**) PL spectra of the CFA fluorescent sensor with Co2+ ions in comparison with a solution without the presence of heavy metal ions (dashed line), (**c**) PL spectra of the solution after removing the CFA fluorescent sensor, (**d**) PL spectra of the solution after adding a new portion of CFA sensor in comparison with a solution without the presence of heavy metal ions (dashed line).

This result suggests that the microspheres successfully absorb the heavy metal ions in solution, which might be concentrated by the magnetic field e.g., further analytical and (micro)biological applications in flow cytometry.

4. Conclusions

In this work, we obtained a sensor based on a porous matrix, which is microspheres of calcium carbonate doped by magnetic Fe_3O_4 nanoparticles and luminescent $AgInS_2$/ZnS QDs. The magnetic properties of Fe_3O_4 and photoluminescent properties of QDs $AgInS_2$/ZnS were combined, yielding highly magnetic and luminescent calcium carbonate microspheres as magneto-fluorescent sensors of heavy metal ions in aqueous solutions. To demonstrate the potential of sensors for sensitivity to in heavy metal ions, the microspheres $CaCO_3$-Fe_3O_4-$AgInS_2$/ZnS were placed in aqueous solutions containing Co^{2+}, Ni^{2+}, and Pb^{2+} ions with various concentrations. By measuring the quenching the PL of the sensor in the presence of heavy metal ions, we demonstrated the possibility of metal ions detection down to a concentration of 10^{-8} M Co^{2+} and 10^{-7} M Ni^{2+}, and Pb^{2+} (≈0.01 ppm, ≈0.1 ppm, and ≈0.1 ppm, respectively).

The main distinguishing feature of the proposed sensor from the luminescent sensors previously reported, e.g., [50,51] is the presence of magnetic properties; therefore, in this work, we also demonstrate the ability to concentrate and remove the sensor from the analyzed system together with ions of the analyzed metals for their precise identification, for example, by the inductively coupled plasma mass spectrometry. These concentrations of ions, which could cause a statistically significant quenching of sensors PL, are much lower than their maximum allowable concentration in natural water. It opens prospects of $CaCO_3$-Fe_3O_4-$AgInS_2$/ZnS sensors for developing methods for the environmental monitoring of heavy metal ions.

Author Contributions: Formal analysis, P.D.K.; Investigation, D.A.K. and P.D.K.; Project administration, A.D., A.V.F. and A.V.B.; Visualization, D.A.K. and M.A.B.; Writing—original draft, D.A.K. and A.D.; Writing—review and editing, A.V.B. and A.V.R. All authors have read and agreed to the published version of the manuscript.

Funding: This research was funded by the Federal Target Program for Research and Development of the Ministry of Science and Higher Education of the Russian Federation (Agreement (No. 14.587.21.0047, identifier RFMEFI58718X0047).

Conflicts of Interest: The authors declare no conflict of interest.

References

1. Roy-Chowdhury, A.; Datta, R.; Sarkar, D. Heavy metal pollution and remediation. In *Green Chemistry*; Elsevier: Amsterdam, The Netherlands, 2018; Volume 94, pp. 359–373.
2. Hembrom, S.; Singh, B.; Gupta, S.K.; Nema, A.K. A comprehensive evaluation of heavy metal contamination in foodstuff and associated human health risk: A global perspective. In *Contemporary Environmental Issues and Challenges in Era of Climate Change*; Singh, P., Singh, R.P., Srivastava, V., Eds.; Springer: Singapore, 2020; pp. 33–63. ISBN 978-981-32-9594-0.
3. Dubey, S.; Shri, M.; Gupta, A.; Rani, V.; Chakrabarty, D. Toxicity and detoxification of heavy metals during plant growth and metabolism. *Environ. Chem. Lett.* **2018**, *16*, 1169–1192. [CrossRef]
4. Mallampati, S.R.; Mitoma, Y.; Okuda, T.; Sakita, S.; Kakeda, M. Total immobilization of soil heavy metals with nano-Fe/Ca/CaO dispersion mixtures. *Environ. Chem. Lett.* **2013**, *11*, 119–125. [CrossRef]
5. Taseidifar, M.; Makavipour, F.; Pashley, R.M.; Rahman, A.F.M.M. Removal of heavy metal ions from water using ion flotation. *Environ. Technol. Innov.* **2017**, *8*, 182–190. [CrossRef]
6. Luo, X.; Lei, X.; Cai, N.; Xie, X.; Xue, Y.; Yu, F. Removal of heavy metal ions from water by magnetic cellulose-based beads with embedded chemically modified magnetite nanoparticles and activated carbon. *ACS Sustain. Chem. Eng.* **2016**, *4*, 3960–3969. [CrossRef]
7. Buledi, J.A.; Amin, S.; Haider, S.I.; Bhanger, M.I.; Solangi, A.R. A review on detection of heavy metals from aqueous media using nanomaterial-based sensors. *Environ. Sci. Pollut. Res.* **2020**, 1–9. [CrossRef]
8. Ullah, N.; Mansha, M.; Khan, I.; Qurashi, A. Nanomaterial-based optical chemical sensors for the detection of heavy metals in water: Recent advances and challenges. *TrAC Trends Anal. Chem.* **2018**, *100*, 155–166. [CrossRef]
9. Liu, Y.; Deng, Y.; Dong, H.; Liu, K.; He, N. Progress on sensors based on nanomaterials for rapid detection of heavy metal ions. *Sci. China Chem.* **2017**, *60*, 329–337. [CrossRef]
10. Kunkel, R.; Manahan, S.E. Atomic absorption analysis of strong heavy metal chelating agents in water and waste water. *Anal. Chem.* **1973**, *45*, 1465–1468. [CrossRef] [PubMed]
11. POHL, P. Determination of metal content in honey by atomic absorption and emission spectrometries. *TrAC Trends Anal. Chem.* **2009**, *28*, 117–128. [CrossRef]
12. Bua, D.G.; Annuario, G.; Albergamo, A.; Cicero, N.; Dugo, G. Heavy metals in aromatic spices by inductively coupled plasma-mass spectrometry. *Food Addit. Contam. Part B* **2016**, *9*, 210–216. [CrossRef] [PubMed]
13. Habila, M.A.; ALOthman, Z.A.; El-Toni, A.M.; Soylak, M. Combination of syringe-solid phase extraction with inductively coupled plasma mass spectrometry for efficient heavy metals detection. *CLEAN-Soil Air Water* **2016**, *44*, 720–727. [CrossRef]
14. Privett, B.J.; Shin, J.H.; Schoenfisch, M.H. Electrochemical sensors. *Anal. Chem.* **2010**, *82*, 4723–4741. [CrossRef] [PubMed]

15. Root, H.D.; Thiabaud, G.; Sessler, J.L. Reduced texaphyrin: A ratiometric optical sensor for heavy metals in aqueous solution. *Front. Chem. Sci. Eng.* **2020**, *14*, 19–27. [CrossRef]
16. Rudd, N.D.; Wang, H.; Fuentes-Fernandez, E.M.A.; Teat, S.J.; Chen, F.; Hall, G.; Chabal, Y.J.; Li, J. Highly efficient luminescent metal–organic framework for the simultaneous detection and removal of heavy metals from water. *ACS Appl. Mater. Interfaces* **2016**, *8*, 30294–30303. [CrossRef]
17. Lou, Y.; Zhao, Y.; Chen, J.; Zhu, J.J. Metal ions optical sensing by semiconductor quantum dots. *J. Mater. Chem. C* **2014**, *2*, 595–613. [CrossRef]
18. Devi, P.; Rajput, P.; Thakur, A.; Kim, K.H.; Kumar, P. Recent advances in carbon quantum dot-based sensing of heavy metals in water. *TrAC-Trends Anal. Chem.* **2019**, *114*, 171–195. [CrossRef]
19. Chaniotakis, N.; Buiculescu, R. Semiconductor quantum dots in chemical sensors and biosensors. In *Nanosensors for Chemical and Biological Applications: Sensing with Nanotubes, Nanowires and Nanoparticles*; Woodhead Publishing: Sawston, UK, 2014; ISBN 9780857096609.
20. Bach, L.G.; Nguyen, T.D.; Thuong, N.T.; Van, H.T.T.; Lim, K.T. Glutathione capped cdse quantum dots: synthesis, characterization, morphology, and application as a sensor for toxic metal ions. *J. Nanosci. Nanotechnol.* **2019**, *19*, 1192–1195. [CrossRef]
21. Zhang, K.; Guo, J.; Nie, J.; Du, B.; Xu, D. Ultrasensitive and selective detection of Cu2+ in aqueous solution with fluorescence enhanced CdSe quantum dots. *Sens. Actuators B Chem.* **2014**, *190*, 279–287. [CrossRef]
22. Vázquez-González, M.; Carrillo-Carrion, C. Analytical strategies based on quantum dots for heavy metal ions detection. *J. Biomed. Opt.* **2014**, *19*, 101503. [CrossRef]
23. Raevskaya, A.; Lesnyak, V.; Haubold, D.; Dzhagan, V.; Stroyuk, O.; Gaponik, N.; Zahn, D.R.T.; Eychmüller, A. A fine size selection of brightly luminescent water-soluble Ag–In–S and Ag–In–S/ZnS quantum dots. *J. Phys. Chem. C* **2017**, *121*, 9032–9042. [CrossRef]
24. Jain, S.; Bharti, S.; Bhullar, G.K.; Tripathi, S.K. I-III-VI core/shell QDs: Synthesis, characterizations and applications. *J. Lumin.* **2020**, *219*, 116912. [CrossRef]
25. Stroyuk, O.; Weigert, F.; Raevskaya, A.; Spranger, F.; Würth, C.; Resch-Genger, U.; Gaponik, N.; Zahn, D.R.T. Inherently broadband photoluminescence in Ag–In–S/ZnS quantum dots observed in ensemble and single-particle studies. *J. Phys. Chem. C* **2019**, *123*, 2632–2641. [CrossRef]
26. Cambrea, L.R.; Yelton, C.A.; Meylemans, H.A. ZnS-AgInS2 fluorescent nanoparticles for low level metal detection in water. In *ACS Symposium Series*; American Chemical Society: Washington, USA, 2015; Volume 1210, ISBN 9780841231092.
27. Baimuratov, A.S.; Rukhlenko, I.D.; Noskov, R.E.; Ginzburg, P.; Gun'ko, Y.K.; Baranov, A.V.; Fedorov, A.V. Giant optical activity of quantum dots, rods and disks with screw dislocations. *Sci. Rep.* **2015**, *5*, 14712. [CrossRef] [PubMed]
28. Stroyuk, O.; Raevskaya, A.; Spranger, F.; Selyshchev, O.; Dzhagan, V.; Schulze, S.; Zahn, D.R.T.; Eychmüller, A. Origin and dynamics of highly efficient broadband photoluminescence of aqueous glutathione-capped size-selected Ag–In–S quantum dots. *J. Phys. Chem. C* **2018**, *122*, 13648–13658. [CrossRef]
29. Podgurska, I.; Rachkov, A. Influence of ions of heavy metals on the photoluminescence of nanocrystals AgInS2 /ZnS. *Sens. Electron. Microsyst. Technol.* **2017**, *14*, 41–47. [CrossRef]
30. Liu, Y.; Zhu, T.; Deng, M.; Tang, X.; Han, S.; Liu, A.; Bai, Y.; Qu, D.; Huang, X.; Qiu, F. Selective and sensitive detection of copper(II) based on fluorescent zinc-doped AgInS2 quantum dots. *J. Lumin.* **2018**, *201*, 182–188. [CrossRef]
31. Podgurska, I.; Rachkov, A.; Borkovska, L. Effect of Pb 2+ ions on photoluminescence of ZnS-coated AgInS 2 nanocrystals. *Phys. Status Solidi* **2018**, *215*, 1700450. [CrossRef]
32. Mokadem, Z.; Mekki, S.; Saïdi-Besbes, S.; Agusti, G.; Elaissari, A.; Derdour, A. Triazole containing magnetic core-silica shell nanoparticles for Pb 2+, Cu 2+ and Zn 2+ removal. *Arab. J. Chem.* **2017**, *10*, 1039–1051. [CrossRef]
33. Zhao, Y.; Lu, Y.; Hu, Y.; Li, J.-P.; Dong, L.; Lin, L.-N.; Yu, S.-H. Synthesis of superparamagnetic CaCO3 mesocrystals for multistage delivery in cancer therapy. *Small* **2010**, *6*, 2436–2442. [CrossRef]
34. Du, C.; Shi, J.; Shi, J.; Zhang, L.; Cao, S. PUA/PSS multilayer coated CaCO3 microparticles as smart drug delivery vehicles. *Mater. Sci. Eng. C* **2013**, *33*, 3745–3752. [CrossRef]
35. Gusliakova, O.; Atochina-Vasserman, E.N.; Sindeeva, O.; Sindeev, S.; Pinyaev, S.; Pyataev, N.; Revin, V.; Sukhorukov, G.B.; Gorin, D.; Gow, A.J. Use of submicron vaterite particles serves as an effective delivery vehicle to the respiratory portion of the lung. *Front. Pharmacol.* **2018**, *9*. [CrossRef] [PubMed]

36. Sha, F.; Zhu, N.; Bai, Y.; Li, Q.; Guo, B.; Zhao, T.; Zhang, F.; Zhang, J. Controllable synthesis of various CaCO 3 morphologies based on a CCUS idea. *ACS Sustain. Chem. Eng.* **2016**, *4*, 3032–3044. [CrossRef]
37. Parakhonskiy, B.; Zyuzin, M.V.; Yashchenok, A.; Carregal-Romero, S.; Rejman, J.; Möhwald, H.; Parak, W.J.; Skirtach, A.G. The influence of the size and aspect ratio of anisotropic, porous CaCO3 particles on their uptake by cells. *J. Nanobiotechnology* **2015**, *13*, 53. [CrossRef] [PubMed]
38. Wei, W.; Ma, G.-H.; Hu, G.; Yu, D.; Mcleish, T.; Su, Z.-G.; Shen, Z.-Y. Preparation of hierarchical hollow CaCO 3 particles and the application as anticancer drug carrier. *J. Am. Chem. Soc.* **2008**, *130*, 15808–15810. [CrossRef]
39. Boyjoo, Y.; Pareek, V.K.; Liu, J. Synthesis of micro and nano-sized calcium carbonate particles and their applications. *J. Mater. Chem. A* **2014**, *2*, 14270–14288. [CrossRef]
40. Dunnick, J.K.; Elwell, M.R.; Radovsky, A.E.; Benson, J.M.; Hahn, F.F.; Nikula, K.J.; Barr, E.B.; Hobbs, C.H. Comparative carcinogenic effects of nickel subsulfide, nickel oxide, or nickel sulfate hexahydrate chronic exposures in the lung. *Cancer Res.* **1995**, *55*, 5251–5256.
41. Thomson, R.M.; Parry, G.J. Neuropathies associated with excessive exposure to lead. *Muscle Nerve* **2006**, *33*, 732–741. [CrossRef]
42. Fathy, M.; Zayed, M.A.; Moustafa, Y.M. Synthesis and applications of CaCO3/HPC core–shell composite subject to heavy metals adsorption processes. *Heliyon* **2019**, *5*, e02215. [CrossRef]
43. Delcea, M.; Möhwald, H.; Skirtach, A.G. Stimuli-responsive LbL capsules and nanoshells for drug delivery. *Adv. Drug Deliv. Rev.* **2011**, *63*, 730–747. [CrossRef]
44. Marchenko, I.; Yashchenok, A.; Borodina, T.; Bukreeva, T.; Konrad, M.; Möhwald, H.; Skirtach, A. Controlled enzyme-catalyzed degradation of polymeric capsules templated on CaCO3: Influence of the number of LbL layers, conditions of degradation, and disassembly of multicompartments. *J. Control. Release* **2012**, *162*, 599–605. [CrossRef]
45. Martynenko, I.V.; Kusić, D.; Weigert, F.; Stafford, S.; Donnelly, F.C.; Evstigneev, R.; Gromova, Y.; Baranov, A.V.; Rühle, B.; Kunte, H.-J.; et al. Magneto-fluorescent microbeads for bacteria detection constructed from superparamagnetic Fe3O4 nanoparticles and AIS/ZnS quantum dots. *Anal. Chem.* **2019**, *91*, 12661–12669. [CrossRef] [PubMed]
46. Hamanaka, Y.; Ogawa, T.; Tsuzuki, M.; Kuzuya, T. Photoluminescence properties and its origin of AgInS 2 quantum dots with chalcopyrite structure. *J. Phys. Chem. C* **2011**, *115*, 1786–1792. [CrossRef]
47. Chen, J.; Zheng, A.; Gao, Y.; He, C.; Wu, G.; Chen, Y.; Kai, X.; Zhu, C. Functionalized CdS quantum dots-based luminescence probe for detection of heavy and transition metal ions in aqueous solution. *Spectrochim. Acta Part A Mol. Biomol. Spectrosc.* **2008**, *69*, 1044–1052. [CrossRef] [PubMed]
48. Baranov, A.V.; Orlova, A.O.; Maslov, V.G.; Toporova, Y.A.; Ushakova, E.V.; Fedorov, A.V.; Cherevkov, S.A.; Artemyev, M.V.; Perova, T.S.; Berwick, K. Dissociative CdSe/ZnS quantum dot-molecule complex for luminescent sensing of metal ions in aqueous solutions. *J. Appl. Phys.* **2010**, *108*, 074306. [CrossRef]
49. Shar, G.A.; Soomro, G.A. Spectrophotometric determination of cobalt (ii), nickel (ii) and copper (ii) with 1-(2 pyridylazo)-2-naphthol in micellar medium. *Nucleus* **2004**, *41*, 77–82.
50. Mahapatra, N.; Panja, S.; Mandal, A.; Halder, M. A single source-precursor route for the one-pot synthesis of highly luminescent CdS quantum dots as ultra-sensitive and selective photoluminescence sensor for Co 2+ and Ni 2+ ions. *J. Mater. Chem. C* **2014**, *2*, 7373. [CrossRef]
51. Parani, S.; Oluwafemi, O.S. Selective and sensitive fluorescent nanoprobe based on AgInS 2 -ZnS quantum dots for the rapid detection of Cr (III) ions in the midst of interfering ions. *Nanotechnology* **2020**, *31*, 395501. [CrossRef]